Philosophical Magazine

ISSN: 1478-6435 (Print) 1478-6443 (Online) Journal homepage: http://www.tandfonline.com/loi/tphm20

# Amorphous silicon hexaboride: a first-principles study

Murat Durandurdu

**To cite this article:** Murat Durandurdu (2018): Amorphous silicon hexaboride: a first-principles study, Philosophical Magazine, DOI: 10.1080/14786435.2018.1503425

**To link to this article:** https://doi.org/10.1080/14786435.2018.1503425

Published online: 29 Jul 2018.

PHILOSOPHICAL MAGAZINE
https://doi.org/10.1080/14786435.2018.1503425

Taylor & Francis
Taylor & Francis Group



# Amorphous silicon hexaboride: a first-principles study

Murat Durandurdu

Department of Materials Science & Nanotechnology Engineering, Abdullah Gül University, Kayseri, Turkey

**ABSTRACT**

We report for the first time the atomic structure, electronic structure and mechanical properties of amorphous silicon hexaboride (*a*-$SiB_6$) based on first-principles molecular dynamics simulation. The *a*-$SiB_6$ model is generated from the melt and predominantly consists of pentagonal pyramid-like configurations and $B_{12}$ icosahedral molecules, similar to what has been observed in most boron-rich materials. The mean coordination number of B and Si atoms are 5.47 and 4.55, respectively. The model shows a semiconducting behaviour with a theoretical bandgap energy of 0.3 eV. The conduction tail states are found to be highly localised and hence the n-type doping is suggested to be more difficult than the p-type doping for *a*-$SiB_6$. The bulk modulus and Vickers hardness of *a*-$SiB_6$ are estimated to be about 118 and 13–17 GPa, respectively.

**ARTICLE HISTORY**
Received 23 April 2018
Accepted 16 July 2018

**KEYWORDS**
Ab initio; amorphous materials; disordered systems

## 1. Introduction

Silicon hexaboride ($SiB_6$) has been attracting considerable attention because of its unique properties such as excellent chemical resistance, high hardness, high thermal stability, excellent electrical conductivity, low thermal conductivity, high melting point, etc. [1–6]. Therefore, it can be used as refractory, thermoelectric and structural materials [1–6].

$SiB_6$ crystal was first synthesised in 1900 [7]. Based on the X-ray structure analysis, in 1956, Zhuravlev suggested a cubic $SiB_6$ crystal having $Pm\bar{3}m$ symmetry similar to $CaB_6$ [8]. Yet, later studies on single crystal could not confirm the cubic phase and instead proposed an orthorhombic state with space group *Pnn2* or *Pnnm* [9–12]. Adamsky [9] postulated an orthorhombic structure (Pnnm) resembling the $B_4C$ type. Giese [11] reported a structure having about 300 atoms in the unit cell. Vlasse et al. [13] proposed a complex structure consisting of 43 Si atoms and 238 B atoms in its orthorhombic unit cell having *Pnnm* symmetry. Theoretical studies [14] based on first-principles calculations and CALYPSO structure prediction methodology suggested

**CONTACT** Murat Durandurdu mdurandurdu@gmail.com Department of Materials Science & Nanotechnology Engineering, Abdullah Gül University, Kayseri 38039, Turkey

several candidates having monoclinic P21/m-type and hexagonal R3m-type structures for $SiB_6$. Consequently, the crystal structure and the atomic positions of $SiB_6$ still remain a mystery.

Amorphous boron (B) rich boron-silicon systems are also of interest and have been considered in some experiments [15,16]. The Raman spectra of amorphous $SiB_6$ (*a*-$SiB_6$) has been also reported [17] but in that study, no information has been provided about its atomic structure. In the present investigation, we report, for the first time, the atomic structure, electronic structure and mechanical properties of *a*-$SiB_6$ using first-principles molecular dynamics (MD) simulations. We find that the key structural unit of the amorphous network is the pentagonal pyramid-like motifs and $B_{12}$ icosahedral molecules similar to ones in most B-rich materials. Our *a*-$SiB_6$ model is a semiconductor with small bandgap energy. The conduction band tail states are projected to be localised and hence p-type doping is much easier than n-type doping. Our calculated mechanical properties are comparable with those of B-rich Si-B crystals.

## 2. Method

In order to generate an *a*-$SiB_6$ model, we used the SIESTA ab initio code [18] within the pseudopotential approach [19] and generalised gradient approximation [20,21]. We selected DZ basis sets and Γ point for the Brillion zone integration. The MD calculations were achieved by the NPT ensemble using the velocity scaling and the Parrinello-Rahman [22] techniques to control temperature and pressure, correspondingly. The time step was set to be 1.0 fs. We used a cubic $SiB_6$ phase with $Pm\bar{3}m$ symmetry as a starting structure having 189 atoms (162 B atoms and 27 Si atoms). This initial crystal structure was subjected to 2000 K for 30 ps and then well equilibrated this liquid state was gradually quenched to 300 K in 100 ps. Finally, the configuration was relaxed using an NPH ensemble till the highest force was less than 0.02 eV/Å. The density of the optimised amorphous structure is 2.2 g/cm$^3$, which is comparable with 2.42 and 2.44 g/cm$^3$ reported for the crystalline samples having B/Si = 6:0(4) and 5.73, respectively [13].

## 3. Results

### 3.1. Atomic structure

The atomic structure of *a*-$SiB_6$ is first identified by the partial pair distribution functions analysis that is provided in Figure 1. The Si-Si correlation presents considerable large fluctuations that are probably associated with statistical noise which originates from a low concentration of Si atoms [23]. According to the analysis of B-B and B-Si correlations, the model presents no long-range order since there is no clear peak beyond 7.0 Å and these correlations approach

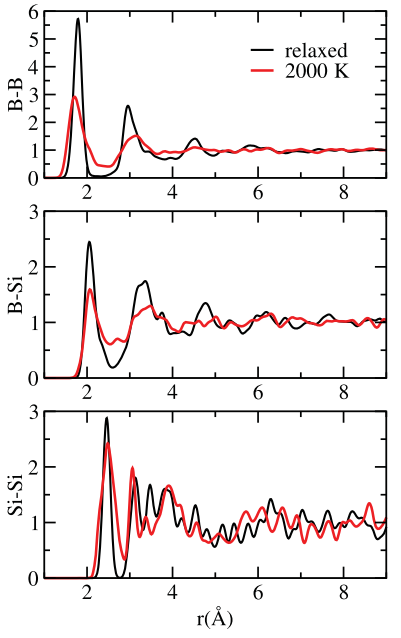


**Figure 1.** Partial pair distribution functions of amorphous and liquid $SiB_6$.

to one. The first, second and third peaks of the B-B correlation are positioned at 1.79 Å, 2.95 Å and 4.52 Å, respectively, which are comparable with the experimental results of 1.78 Å, 3.02 Å and 4.54 Å reported for amorphous boron [24] and of 1.76 Å, 3.15 Å and 4.7 Å found for the liquid boron at 2600 K (1.78 Å, 3.15 Å, and 4.7 Å at 2400 K) [25]. Additionally, the estimated average B-B bond length (1.79 Å) is also comparable with the mean B-B distance of 1.773 Å in $SiB_6$ [13]. The first three peaks of B-Si correlation are placed at 2.05 Å, 3.36 Å and 4.77 Å. Again the Si-B bond distance projected is in the range of experimental suggestions of 1.98–2.13 Å in $SiB_6$ [13]. On the other hand, the mean Si-Si bond length is measured to be 2.46 Å, which is quite larger than the experimental predictions of 2.12–2.21 Å in $SiB_6$ [13] and 2.35 Å in the elemental Si crystal. The pronounced second and third coordination shells might be inferred as the presence of a medium-range order in *a*-$SiB_6$, which is probably due to the pentagonal pyramid-like motifs and $B_{12}$ icosahedral molecules.

Once the amorphous and liquid states are compared, one can see that the position of most peaks (first, second or third) in the liquid state is slightly different than those of *a*-$SiB_6$ (see Figure 1), suggesting that the bonding distances are not sensitive to temperature. Yet, as expected the peaks become more pronounced after the liquid state is solidified.

Using the first minimum of the correlation functions (B-B = 2.1 Å, B-Si = 2.6 Å and Si-Si = 2.77 Å), we estimate partial coordination numbers, the coordination distribution of each species and chemical environmental distribution of

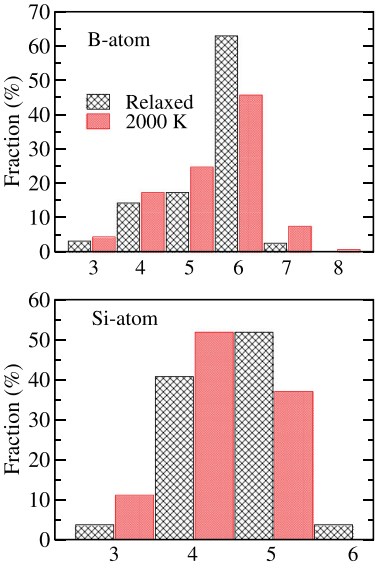


**Figure 2.** Coordination distribution of B and Si atoms.

each atom in our *a*-$SiB_6$ model. The mean coordination number of B and Si atoms are projected to be 5.47 and 4.55, respectively. As seen in Figure 2, the six-fold coordinated B atoms are the most privileged one with a frequency of about 63%. The fraction of four-fold and five-fold coordinated units is 14% and 17%, correspondingly. For Si atoms, the most dominated clusters are the four-fold (41%) and five-fold (52%) coordinated motifs. In the $SiB_3$ crystal, all B atoms are six-fold coordinated while Si atoms are five-fold coordinated. For the case of the $SiB_4$ phase, again B atoms are six-fold coordinated whereas Si atoms form both two-fold and four-fold coordination, yielding mean coordination number of Si atoms to be 3.33. So one can see that the predicted partial coordination numbers of *a*-$SiB_6$ are in the expected ranges considering its disordered nature. The chemical environmental distributions of B and Si atoms are given in Table 1. The most dominated clusters around B atoms are B-$B_6$ and B-$B_5$Si clusters, which are ideal pentagonal pyramid-like configurations (see below). The five-fold coordinated B atoms show generally the typical incomplete pentagonal pyramid-like motifs (see below). The environment of Si atoms appears to be slightly complicated than B atoms and four different types of clusters are privileged ones in the model, which are Si-$B_5$, Si-$B_4$, Si-$B_4$Si and Si-$B_3$Si. The five-fold coordinated motifs (Si-$B_5$, and Si-$B_4$Si) arrangements are the incomplete pentagonal pyramid-like clusters as well. The tetrahedrally coordinated atoms do not represent the ideal tetrahedron structure and hence their angles deviate from 109.5°.

In the liquid state, the average coordination number of B and Si atoms are projected to be 5.35 and 4.25, respectively. As understood from Figure 2, B atoms form less six-fold coordinated structures in the liquid state. Also, Si

**Table 1.** Chemical identities around B and Si atoms.

| Relaxed | | | | 2000 K | | | |
|---|---|---|---|---|---|---|---|
| B | | Si | | B | | Si | |
| $B_6$ | 41.358% | $B_5$ | 25.926% | $B_6$ | 32.099% | $B_5$ | 14.815% |
| $B_5Si_1$ | 18.519% | $B_4$ | 22.222% | $B_5Si_1$ | 12.963% | $B_4$ | 11.111% |
| $B_4Si_1$ | 8.642% | $B_4Si_1$ | 18.519% | $B_4Si_1$ | 6.173% | $B_4Si_1$ | 11.111% |
| $B_3Si_1$ | 4.938% | $B_3Si_1$ | 14.815% | $B_3Si_1$ | 8.025% | $B_3Si_1$ | 29.630% |
| $B_3Si_2$ | 4.321% | $B_3Si_2$ | 7.407% | $B_3Si_2$ | 6.173% | $B_3Si_2$ | 7.407% |
| $B_4$ | 4.321% | $B_4Si_2$ | 3.704% | $B_4$ | 6.173% | $B_4Si_2$ | 0.0% |
| $B_5$ | 3.704% | $B_2Si_1$ | 3.704% | $B_5$ | 11.728% | $B_2Si_1$ | 3.704% |
| $B_4Si_2$ | 3.086% | $B_2Si_2$ | 3.704% | $B_4Si_2$ | 0.617% | $B_2Si_2$ | 7.407% |
| $B_1Si_3$ | 2.469% | | | $B_1Si_3$ | 0.0% | $B_3$ | 3.704% |
| $B_2Si_2$ | 2.469% | | | $B_2Si_2$ | 3.086% | $B_1Si_3$ | 3.704% |
| $B_2Si_1$ | 1.852% | | | $B_2Si_1$ | 2.469% | $B_2Si_3$ | 3.704% |
| $B_7$ | 1.852% | | | $B_7$ | 4.938% | $B_1Si_2$ | 3.704% |
| $B_3$ | 0.617% | | | $B_3$ | 1.852% | | |
| $B_2Si_3$ | 0.617% | | | $B_2Si_3$ | 0.617% | | |
| $B_6Si_1$ | 0.617% | | | $B_6Si_1$ | 2.469% | | |
| $B_1Si_2$ | 0.617% | | | $B_1Si_2$ | 0.0% | | |

atoms form more four-fold coordinated units than five-fold coordinated units in the liquid state. Nonetheless, there is no so drastic difference between the liquid and amorphous states when the coordination numbers are considered.

The Voronoi polyhedra approach is used to shed light onto the short range order of *a*-$SiB_6$. A Voronoi polyhedron is symbolised by the indices $\langle v_3, v_4, v_5, v_6, \ldots \rangle$, where $v_i$ and $\sum v_i$ correspond to the number of i-edge faces of a polyhedron and the coordination number, respectively. B atoms in the amorphous model present seven distinctive polyhedra and the most frequent ones are represented by the <2, 2, 2, 0> (62%), <2, 3, 0, 0> (16%) and <4, 0, 0, 0> (12%) indices. The most dominant clusters for Si atoms are, on the other hand, signified by the <2, 3, 0, 0> (48%) and <4, 0, 0, 0> (40%) indices. The <2, 2, 2, 0> type clusters for Si atoms are negligibly small. The <2, 2, 2, 0> and <2, 3, 0, 0> type polyhedrons are related to the ideal and incomplete pentagonal pyramids as shown in Figure 3. The <4, 0, 0, 0> type polyhedral can be considered as incomplete pentagonal pyramids as well (see Figure 3). The ideal and incomplete pentagonal pyramids lead to the formation of complete or incomplete $B_{12}$ icosahedrons in the amorphous network as illustrated in Figure 4.

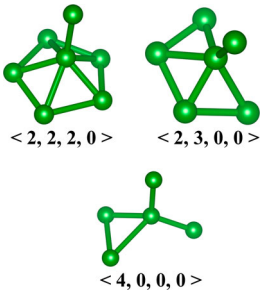


**Figure 3.** Most dominated Voronoi clusters for B atoms. Si atoms also show the similar type of polyhedrons.

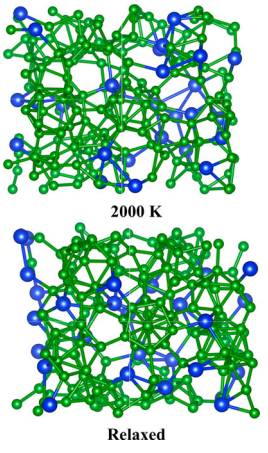


**Figure 4.** Ball-stick representation of liquid $SiB_6$ and relaxed *a*-$SiB_6$.

Bond angle distribution analysis illustrated in Figure 5 can provide information in details at the atomistic level. The B-B-B distribution possesses two peaks at around 60° and 108°. These angles are indeed comparable with the angles of 60° and 108° originated from the intra-icosahedral bonds of the pentagonal pyramids (the quasimolecular $B_{12}$ icosahedron). The general shape of the B-B-B angle distribution function is actually quite similar to what has been reported for *a*-B and liquid B. The Si-Si-Si angles have two peaks at 90° and 105°. The B-Si-B (Si-B-Si) angles have a broad distribution ranging from 40° to 150°. This is due to the contribution of different types of Si clusters (Si-$B_5$, Si-$B_4$, Si-$B_4$Si and Si-$B_3$Si) to the angles distributions.

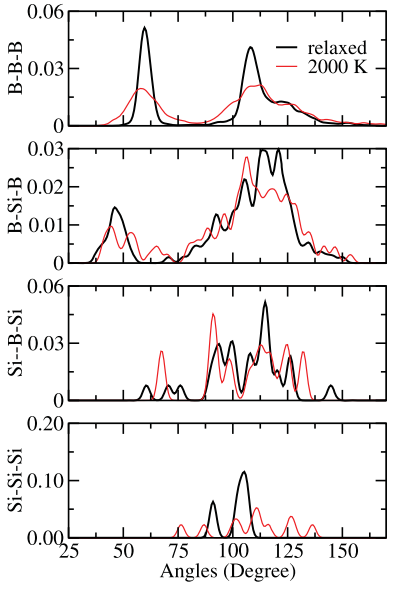


**Figure 5.** Bond angle distribution of amorphous and liquid $SiB_6$.

The bond angle distributions of the liquid $SiB_6$ are quite similar to those of *a*-$SiB_6$ and show peaks almost at the same angles except the Si-Si-Si angles that range 75° and 135°. This finding means that the liquid and amorphous states are structurally close to each other. Yet a visual review of the structures reveals that the main structural difference between the liquid state and *a*-$SiB_6$ is the lack of the $B_{12}$ molecules in the liquid state.

### 3.2. Electronic structure

The electronic properties of *a*-$SiB_6$ are analysed by examining the electron density of states (EDOS), partial density of states (PDOS) and localisation of eigenstates. The EDOS given in Figure 6 shows semi-metallic-like character due to the small bandgap energy projected in the simulation. The estimated HOMO–LUMO bad gap is 0.3 eV for *a*-$SiB_6$. This value is unquestionably underestimated due to the limitation of DFT-GGA calculation. In an experimental study, the bandgap energy of B-rich amorphous Si-B systems is predicted to be in the range of 0.5–1.0 eV and to decrease with increasing B concentration. So one can see our bandgap energy is in reasonable limits when it is compared with the experimental values. Additional information can be obtained from PDOS given in Figure 6. As seen from the figure, B-*p* states are the most dominated ones for both valence and conduction bands while the contribution of Si-states to the EDOS is significantly small. This is believed to be a charge transfer from Si atoms to B atoms to stabilise the structure [14]. Similar findings are also reported in B-rich Si-B crystals [14].

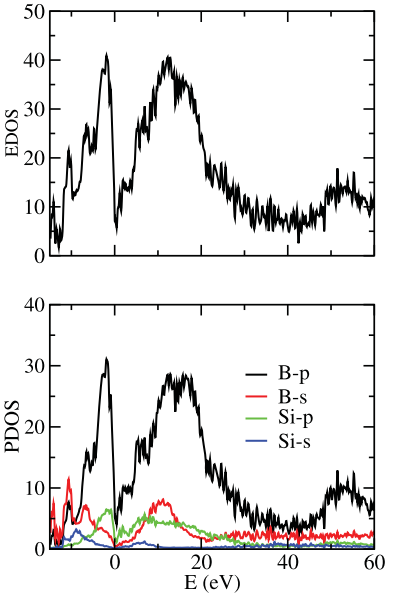


**Figure 6.** EDOS and PDOS of amorphous $SiB_6$.

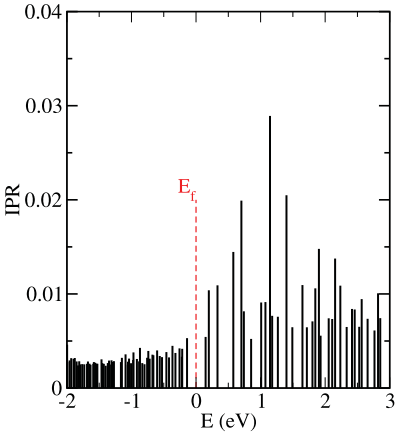


**Figure 7.** IPR near the Fermi level that is located at 0 eV.

We calculate the inverse participation ratio ($IPR(\psi_j) = N\sum_{i=1}^{N} a_i^{j4} / \left(\sum_{i=1}^{N} a_i^{j2}\right)^2$ where $\psi_j = \sum_{i=1}^{N} a_i^j \phi_i$ is the $j^{\text{th}}$ eigenstate and $N$ is the number of atoms, see [26] for additional information) to probe the localisation of eigenstates and hence have further knowledge regarding the electronic structure of $a$-$SiB_6$. The estimated IPR is given in Figure 7. The conduction tails are localised due to their high IPR while the valence tail states are weakly localised due to their low IPR. One can see an asymmetric localisation of the tail states. Using the localisation of tail states, possible distinctions in n-type and p-type doping for a material can be speculated [26,27]. Because of the localisation of the conduction tail states, it would be hard to shift the Fermi level to the conduction band and hence the n-type doping is expected to be harder than p-type doping for $a$-$SiB_6$. High electron mobilities are estimated if the material can be p-type doped.

### 3.3. Mechanical properties

In order to compute bulk modulus ($K$) of the model, we probe its total energy as a function of volume and fit our data to the third-order Birch–Murnaghan equation of states,

$$E(V) = E_0 + \frac{9V_0K}{16}\left\{\left[\left(\frac{V_0}{V}\right)^{\frac{2}{3}} - 1\right]^3 K' + \left[\left(\frac{V_0}{V}\right)^{\frac{2}{3}} - 1\right]^2 \left[6 - 4\left(\frac{V_0}{V}\right)^{\frac{2}{3}}\right]\right\}$$

where $E$ and $V$ are the energy and volume, respectively, $E_0$ and $V_0$ represent their zero pressure values and $K'$ is the derivative of $K$ respect to pressure. The $K$ value is predicted to be about 118 GPa. In a compressive study of B-rich B-Si

crystalline systems ($SiB_3$, $SiB_4$, $SiB_6$, and $SiB_{36}$), the $K$ values are found to be in the range of 121–183 GPa [14]. Considering the disordered nature of the $a$-$SiB_6$ model, our estimation is fairly comparable with them.

To calculate the Poisson's ratio, uniaxial stresses along $x$-, $y$- and $z$-directions of the amorphous model are applied and the variation along transfer directions is examined. The Poisson ratio of a solid subjected to a uniaxial compression is defined as

$$\upsilon_{ij} = -\frac{\Delta L_i/L_i}{\Delta L_j/L_j}$$

where $i$ and $j$ represent the transfer and applied strain directions, respectively and $Ls$ are the magnitude of the diagonal terms of the simulation cell vectors. We estimate the Poisson's ratio using the best linear fitting line and have six different values varying from 0.18 to 0.26 are obtained. The mean Poisson's ratio is 0.2, which is reasonably close to the values of 0.17–0.35 reported for B-rich B-Si crystals [14]. We should note that because of the fitting, we surely expect some errors in our projected Poisson's ratio.

Knowing the $K$ value and the Poisson's ratio ($\nu$) is enough to estimate Young's modulus ($E$) using the following equation:

$$E = 3K(1 - 2\nu)$$

The $E$ value calculated is 212 GPa, which is again comparable with 150–358 predicted for the B-rich B-Si crystals.

We compute the shear modulus ($\mu$) using the next definition

$$\mu = \frac{E}{2(1 + \nu)}$$

Shear modulus of $a$-$SiB_6$ is projected to be 88 GPa, in agreement with the earlier reports of 55–153 GPa [14].

Vickers hardness is predicted using Chen's equation [28],

$$H = 2\left(\frac{\mu}{n^2}\right)^{0.585} - 3(\text{GPa})$$

where $n$ is the Pugh's ratio ($n = K/\mu$) and Teter's equation [29]

$$H = 0.151\mu$$

to be about 17 and 13 GPa, respectively.

Pugh's ratio or Poisson's ratio can be used to classify the brittle-ductile nature of solids [30,31]. The critical value of $n$ is 1.75 and it is greater than 1.75 for ductile solids and smaller than 1.75 for brittle solids. $n$ is 1.33 for $a$-$SiB_6$ suggesting its brittle character. For the Poisson's ratio consideration, if $\nu$ is greater (smaller) than 0.26, then the material is ductile (brittle). The Poisson ration is 0.2 for $a$-$SiB_6$, implying again its brittle nature.

## 4. Conclusions

In the present work, the atomic structure, electronic structure and mechanical properties of an *a*-$SiB_6$ model generated using on first-principles MD simulation are reported for the first time. The main building structure of *a*-$SiB_6$ is found to be the pentagonal pyramid-like units and $B_{12}$ icosahedral molecules as seen in most B-rich materials. The average coordination number of B and Si atoms are 5.47 and 4.55, correspondingly. The model presents 0.3 eV bandgap energy. We see the highly localised conduction tail states and speculate that the p-type doping is easier than the n-type doping. The mechanical properties of *a*-$SiB_6$ are found to be comparable with those of B-rich B-Si crystals.

## Acknowledgements

The simulations were run on the TÜBİTAK ULAKBİM, High Performance and Grid Computing Center (TRUBA resources).

## Disclosure statement

No potential conflict of interest was reported by the author(s).

## Funding

This work was supported by the Scientific and Technological Research Council of Turkey (TÜBİTAK) under grant number 117M372.

## References

[1] S.H. Shim, D.W. Lee, J.H. Chae, J.I. Matsushita, and K.B. Shim, *Thermoelectric characteristics of the spark plasma-sintered silicon boride ceramics*, J. Korean Cryst. Growth Cryst. Techn. 15 (2005), pp. 75–78.

[2] M. Mukaida, T. Tsunoda, and Y. Imai, Preparation of B-Si films by chemical vapor deposition, In Eighteenth International Conference on Thermoelectrics 1999, pp. 667–670. IEEE, 1999.

[3] L. Chen, T. Goto, M. Mukaida, M. Niino, and T. Hirai, *Phase diagram and thermoelectric property of Si-B system ceramics*, J. Jpn. Soc. Powder Powder Metall. 41 (1994), pp. 1299–1303.

[4] J. Matsushita and S. Komarneni, *High temperature oxidation of silicon hexaboride ceramics*, Mater. Res. Bull. 36, (2001), pp.1083–1089.

[5] G.C. Hwang and J.-Ichi Matsushita, *Preparation of Si infiltrated SiB6-TiB2 composites*, J. Ceram. Process. Res. 11(2010), pp. 1–5.

[6] J. Ichi Matsushita, A. Kitajima, S. Okuhata, K.B. Shim, K.H. Auh, and K. Niihara, *Oxidation behavior of a silicon boride composite*, J. Ceram. Process. Res. 5 (2004), pp. 133–135.

[7] H. Moissan and A. Stock, *Preparation and properties of two silicon borides: SiB3 and SiB6*, CR Acad. Sci. Paris 131 (1900), pp. 139–-143.

[8] N.N. Zhuravlev, *X-ray determination of the structure of SiB*, Kristallografiya 1 (1956), pp. 666–668.

[9] R.F. Adamsky, *Unit cell and space group of orthorhombic SiB6*, Acta Crystallogr. 11 (1958), pp.744–745.
[10] C.F. Cline, *Preliminary investigations of the silicon boride, SiB6*, Nature 181 (1958), pp. 476–477.
[11] R.F. Giese, *Polyhedral groups in the phase SiB6*, Electron. Technol. 3 (1970), pp. 151–157.
[12] E. Lugscheider, H. Reimann, and W.J. Quadakkers, Das system bor-silicium, Berichte der deutschen keramischen gesellschaft 56 (1979), pp. 301–305.
[13] M. Vlasse, G.A. Slack, M. Garbauskas, J.S. Kasper, and J.C. Viala, *The crystal structure of SiB6*, J. Solid State Chem. 63 (1986), pp. 31–45.
[14] B. Zhang, L. Wu, and Z. Li, *Predicted structural evolution and detailed insight into configuration correlation, mechanical properties of silicon–boron binary compounds*, RSC Adv. 7 (2017), pp. 16109–16118.
[15] M. Takeda, M. Ichimura, H. Yamaguchi, Y. Sakairi, and K. Kimura, *Preparation of boron–silicon thin film by pulsed laser deposition and its properties*, J. Solid State Chem. 154 (2000), pp. 141–144.
[16] C.W. Ong, K.P. Chik, and H.K. Wong, *Effects of Si incorporation on the structural change of a-$B_x$ $Si_{1-x}$ alloy films*, J. Appl. Phys. 74 (1993), pp. 6094–6099.
[17] J.S. Lannin and R. Messier, *Low-frequency modes in amorphous boron-rich alloys*, Phys. Rev. Lett. 45 (1980), pp. 1119–1122.
[18] P. Ordejón, E. Artacho, and J.M. Soler, *Self-consistent order-N density-functional calculations for very large systems*, Phys. Rev. B 53 (1996), pp. R10441–R10444.
[19] N. Troullier and J.M. Martins, *Efficient pseudopotentials for plane-wave calculations*, Phys. Rev. B 43 (1991), pp. 1993–2006.
[20] A.D. Becke, *Density-functional exchange-energy approximation with correct asymptotic behavior*, Phys. Rev. A 38 (1988), pp. 3098–3100.
[21] C. Lee, W. Yang, and R.G. Parr, *Development of the Colle-Salvetti correlation-energy formula into a functional of the electron density*, Phys. Rev. B 37 (1988), pp. 785–789.
[22] M. Parrinello and A. Rahman, *Polymorphic transitions in single crystals: a new molecular dynamics method*, J. Appl. Phys. 52 (1981), pp. 7182–7190.
[23] J.K. Christie, *Atomic structure of biodegradable Mg-based bulk metallic glass*, Phys. Chem. Chem. Phys. 17 (2015), pp. 12894–12898.
[24] R.G. Delaplane, T. Lundstrom, U. Dahlborg, and W.S. Howells, in: D. Emin, T.L. Aselage, A.C. Switendick, B. Morosin, C.L. Beckel (Eds.), Boron-Rich Solids, AIP Conf. Proc., No. 231, AIP, New York, 1991, p. 241.
[25] S. Krishnan, S. Ansell, J.J. Felten, K.J. Volin, and D.L. Price, *Structure of liquid boron*, Phys. Rev. Lett. 81 (1998), pp. 586–589.
[26] B. Cai and D.A. Drabold, *Properties of amorphous GaN from first-principles simulations*, Phys. Rev. B 84 (2011), pp. 075216–075221.
[27] J. Robertson, *Physics of amorphous conducting oxides*, J. Non-Cryst. Solids 354 (2008), pp. 2791–2795.
[28] X.Q. Chen, H. Niu, D. Li, and Y. Li, *Modeling hardness of polycrystalline materials and bulk metallic glasses*, Intermetallics 19 (2011), pp. 1275–1281.
[29] D.M. Teter, *Computational alchemy: the search for new superhard materials*. MRS Bull. 23 (1998), pp. 22–27.
[30] G. Vaitheeswaran, V. Kanchana, A. Svane, and A. Delin, *Elastic properties of MgCNi3 – a superconducting perovskite*, J. Phys. Conden. Matter 19 (2007), pp. 326214–326219.
[31] I.N. Frantsevich, F.F. Voronov, S.A. Bokuta, Elastic constants and elastic moduli of metals and insulators handbook, Naukova Dumka, Kiev, 1983, pp. 60–180.